

## Symmetry breaking in clogging for oppositely driven particles

Tobias Glanz, Raphael Wittkowski,\* and Hartmut Löwen

*Institut für Theoretische Physik II: Weiche Materie, Heinrich-Heine-Universität Düsseldorf, D-40225 Düsseldorf, Germany*

(Received 10 November 2015; revised manuscript received 24 June 2016; published 17 November 2016)

The clogging behavior of a symmetric binary mixture of colloidal particles that are driven in opposite directions through constrictions is explored by Brownian dynamics simulations and theory. A dynamical state with a spontaneously broken symmetry occurs where one species is flowing and the other is blocked for a long time, which can be tailored by the size of the constrictions. Moreover, we find self-organized oscillations in clogging and unclogging of the two species. Apart from statistical physics, our results are of relevance for fields like biology, chemistry, and crowd management, where ions, microparticles, pedestrians, or other particles are driven in opposite directions through constrictions.

DOI: [10.1103/PhysRevE.94.052606](https://doi.org/10.1103/PhysRevE.94.052606)

### I. INTRODUCTION

Understanding the flow of particles through patterned channels is of great relevance for fields ranging from nanofluidics [1–4] to medicine [5–7] to crowd management [8] but is also interesting from a fundamental physics point of view. In this regard, the clogging and unclogging behavior near constrictions is of prime importance as it stops and restarts the global flow. This has been explored a lot for a single species of particles driven through a narrow constriction. On the nanoscale, the permeation of molecules through structured pores has been found to be controlled by constrictions [9]. Colloidal particles [10–12], dusty plasmas [13], and micron-sized bacteria [14,15] passing through micropatterned channels constitute microscopic situations where clogging is essential. On the mesoscale, vascular clogging by parasitized red blood cells [16] has been studied, and in the macroscopic world, clogging has been observed in gravity-driven granulates in silos [17,18] and when pedestrians or animals like sheep escape through a narrow door [19–22].

Here we address the clogging behavior of mixtures of two particle species that are driven in opposite directions through channels with constrictions. In the absence of any constrictions, rich pattern formation like laning and banding has been found in many such systems [23–31], but studies on corresponding systems with constrictions are rare [32,33]. This is surprising since there are many real systems where the flow of oppositely driven particles through constrictions is of great importance. An example from the microworld involves oppositely charged ions in an electric field that drives the particles in opposite directions through the pores of a membrane. Such ionic counterflows occur especially in ion channels that are present in the membranes of all cells and that are key components in various biological processes [34]. The proper transport of ions through ion channels is crucial for muscle contraction, T-cell activation, regulation of the cell volume, and many other biochemical processes, and an impairment of ion channel transport (e.g., due to channelopathies) has disastrous consequences for the organism [35]. Ionic counterflows through a porous medium

also occur in gel electrophoresis. An example from the macroworld involves pedestrians who intend to exit and enter a building at the same time through a narrow door [32,33].

In this article we explore the rich flow and clogging behavior of a symmetric binary mixture of oppositely driven particles in a channel with constrictions within a simple two-dimensional model designed for colloidal suspensions. For a completely symmetric situation of an initially homogeneous mixture in a periodic channel with spatial inversion symmetry, we observe states of simultaneous flow and of simultaneous clogging of the two particle species, but interestingly we also find a *spontaneous symmetry breaking* of clogging. This phenomenon implies that although both flow directions are equivalent in the model, one species is flowing and the other species is clogging. The partial clogging can be inverted after a characteristic flipping time  $\tau_1$ , but the flipping time becomes very long if the constrictions are narrow. This means that in the symmetry-broken state the flow of one species dominates on reasonable time scales. Moreover, for narrow constrictions we observe a state of self-organized oscillations in clogging and unclogging of the two species. These effects occur especially in systems with large average particle densities and can be exploited to trigger the partial flow of binary mixtures through patterned channels.

This article is organized as follows: After describing our model in Sec. II, we study it on the basis of computer simulations in Sec. III. This numerical investigation is complemented by theoretical considerations in Sec. IV. In Sec. V we address the relevance of our results by suggesting possible experimental realizations of our model and by discussing the applicability of the model to other systems. Finally, we conclude in Sec. VI.

### II. MODEL

In our model, we consider a channel with sinusoidal walls described by the functions  $w(z) = b/2 + a[1 - \cos(2\pi z/\lambda)]$  and  $-w(z)$ , where  $z$  is the coordinate along the channel axis,  $b$  is the minimal wall distance,  $a$  is the amplitude of the spatial wall modulation, and  $\lambda$  is its period length [see inset in Fig. 1(a)].

This channel confines a colloidal suspension of two species (i.e., a binary mixture) of driven, interacting, spherical Brownian particles with the same particle number and the same effective particle diameter  $\sigma$  (see below). The external driving

\*Present address: Institut für Theoretische Physik, Westfälische Wilhelms-Universität Münster, D-48149 Münster, Germany.

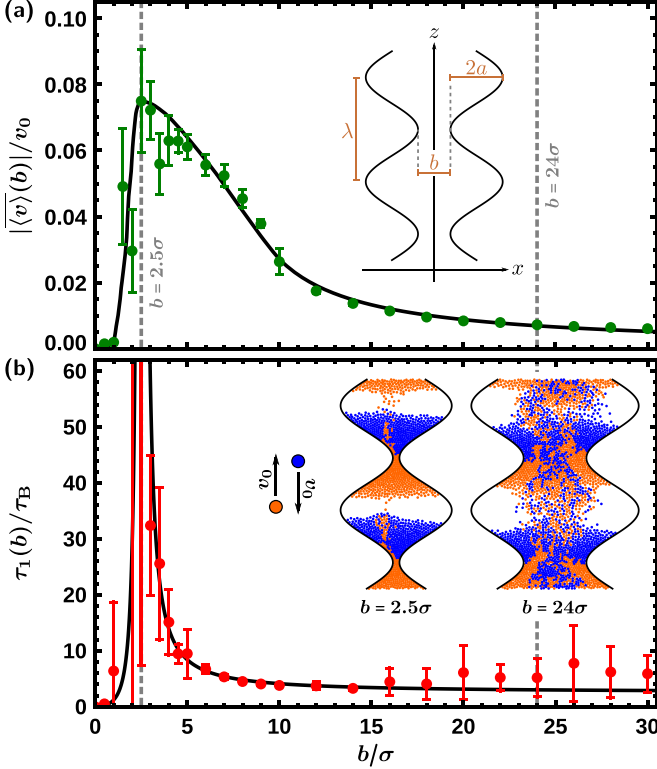


FIG. 1. Dependence of the (a) time-averaged absolute value  $|\langle v \rangle(b)|$  of the mean particle velocity  $\langle v \rangle(b)$  and (b) characteristic flipping time  $\tau_1(b)$  on the minimum wall distance  $b$  for  $\phi = 0.8$ . The points with error bars correspond to 20 simulations each and the black curves are fit curves. Insets: (a) sketch of the channel walls and (b) illustration of the driving directions of the two particle species as well as particle distributions in the asymmetric ( $b = 2.5\sigma$ ) and symmetric ( $b = 24\sigma$ ) flow states.

force has the same absolute value  $F_{\text{ext}}$  for all particles. It drives the particles of one species in the  $z$  direction and the particles of the other species in the opposite direction.

The dynamics of the particles in our model is overdamped. If a particle is not interacting with other particles or with the wall, the external driving force leads to the maximum particle speed  $v_0$ . Such a system is described by the Langevin equations

$$\dot{\mathbf{r}}_i = v_0^{(i)} \hat{\mathbf{e}}_z + \beta D_T [\mathbf{F}_{\text{int}}^{(i)}(\{\mathbf{r}_j\}) + \mathbf{F}_{\text{wall}}(\mathbf{r}_i)] + \sqrt{2D_T} \boldsymbol{\xi}_i, \quad (1)$$

where  $\mathbf{r}_i(t)$  is the position of the  $i$ th particle at time  $t$ .  $v_0^{(i)}$  is equal to  $v_0 = \beta D_T F_{\text{ext}}$  if  $i$  is odd and equal to  $-v_0$  otherwise,  $\hat{\mathbf{e}}_z$  is the unit vector in  $z$  direction,  $\beta = 1/(k_B T)$  is the inverse thermal energy with Boltzmann constant  $k_B$  and absolute temperature  $T$ ,  $D_T$  is the translational diffusion coefficient of a free particle, and the total initial number of particles  $N_\lambda = 4\phi\lambda(b + 2a)/(\pi\sigma^2)$  in a channel segment of length  $\lambda$  is prescribed by a particle packing fraction  $\phi$  [36]. The force  $\mathbf{F}_{\text{int}}^{(i)}(\{\mathbf{r}_j\}) = -\sum_{j \neq i} \nabla_{\mathbf{r}_i} U(\|\mathbf{r}_i - \mathbf{r}_j\|)$  acting on particle  $i$  with the pair-interaction potential  $U(r)$  takes into account interactions with other particles,  $\mathbf{F}_{\text{wall}}(\mathbf{r}) = -\nabla_{\mathbf{r}} U(w(z) - |x|)$  is the force that the wall exerts on a particle at position  $\mathbf{r} = (x, z)$ , and the components of  $\boldsymbol{\xi}_i(t)$  are uncorrelated standard Gaussian white noise terms. To describe the interactions, we used the soft Yukawa potential of point particles  $U(r) = U_0 \exp(-\kappa r)/(\kappa r)$

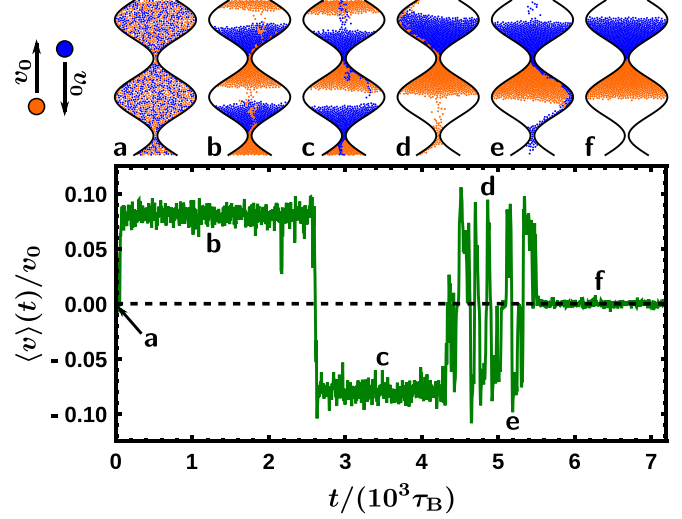


FIG. 2. Time-dependent mean particle velocity  $\langle v \rangle(t)$  and corresponding particle distributions from a simulation with  $b = 2\sigma$  and  $\phi = 0.8$ . (a) Homogeneous random initial distribution, long-lasting (b) forward and (c) backward mean flow, oscillatory state with alternating short-living (d) forward and (e) backward mean flows, and (f) completely jammed state.

modeling charge-stabilized colloids at low volume fractions with  $\kappa = 6/\sigma$ . The parameter  $U_0$  controls the interaction strength and is chosen so that  $-U'(\sigma) = F_{\text{ext}}$ . This equates the repulsive force  $-U'(\sigma)$  on two particles with center-to-center distance  $\sigma$  with the driving force  $F_{\text{ext}}$ , thereby ensuring that the center-to-center distance of two colliding particles cannot exceed the effective particle diameter  $\sigma$ .

### III. COMPUTER SIMULATIONS

To simulate such a system, we solved Eq. (1) numerically employing the Ermak-McCammon scheme [37]. For these Brownian dynamics simulations, we used the effective particle diameter  $\sigma$ , Brownian time  $\tau_B = \sigma^2/D_T$ , and thermal energy  $k_B T$  as units for length, time, and energy, respectively. We considered a channel of length  $2\lambda$  with periodic boundary conditions and used homogeneous random initial particle distributions [see Fig. 2(a)]. Furthermore, we have chosen  $a = 10\sigma$ ,  $\lambda = 40\sigma$ , the Péclet number  $\text{Pe} = v_0\sigma/D_T = 10$ , as well as the time step size  $\Delta t = 10^{-4}\tau_B$  and studied systems with  $0 \leq b \leq 30\sigma$ ,  $0 \leq \phi \leq 1$ , and  $0 \leq t \leq 10^4\tau_B = 10^5\sigma/v_0$ . This means that our simulations involved up to 5092 particles (i.e., 1792 particles for  $b = 2\sigma$  and  $\phi = 0.8$ ; cf. Fig. 2) and that an individual particle with speed  $v_0$  could traverse the channel more than 1000 times within the simulation period.

We found that for large  $b$  the particles of the two species can easily move simultaneously in opposite directions through the constrictions and create a persistent *symmetric flow* with a vanishing mean particle velocity  $\langle v \rangle$  (see inset in Fig. 1(b) and supplemental movies [38]), where  $\langle \cdot \rangle$  denotes an average over all particles at a certain time. In contrast, if  $b$  is sufficiently small, the particles can hardly pass the constrictions and many particles accumulate near them. Interestingly, in such a system, which is initially invariant under parity inversion and time

reversal, a *spontaneous symmetry breaking* can be observed: The particles of one species are passing the constrictions, whereas the motion of the other particles is blocked [39] (see inset in Fig. 1(b) and supplemental movies [38]). In this persistent *asymmetric flow*,  $\langle v \rangle$  is nonzero [see Fig. 2(b)]. When  $b$  becomes smaller, the time-averaged absolute value  $|\overline{\langle v \rangle}(b)|$  of  $\langle v \rangle(b)$  with  $\overline{\phantom{x}}$  denoting an average over time increases; its maximum value can be observed at  $b \approx 2.5\sigma$  [see Fig. 1(a)]. For even smaller  $b$ ,  $|\overline{\langle v \rangle}(b)|$  decreases again, since fewer particles can pass the constrictions in a given time period, until it becomes impossible for particles to pass the constrictions so that  $\langle v \rangle$  is zero. The latter happens for  $0 \leq b \lesssim \sigma$ .

In the asymmetric flow state, the sign of the mean particle velocity  $\langle v \rangle$  is random. After a characteristic flipping time  $\tau_1$  [40], the direction of the asymmetric flow and thus the sign of  $\langle v \rangle$  change [see Fig. 2(c); this can happen several times in succession] or the system proceeds with a different flow state [see Figs. 2(d)–2(f)]. As revealed by Fig. 1(b),  $\tau_1$  is nonmonotonic in  $b$  and can become extremely large near the maximum of  $|\overline{\langle v \rangle}(b)|$ , but decreases for larger and—due to frequent jamming—smaller  $b$ .

After such an asymmetric flow, two other flow states are possible: an oscillatory state [see Figs. 2(d) and 2(e)] and a completely jammed state [see Fig. 2(f)]. Both states have in common that the flow is nearly or completely blocked at one constriction so that the particles accumulate only there. In contrast to the asymmetric flow state, where the continuous particle flow avoids a positional ordering of the particles in the dense regions, in the oscillatory and completely jammed states a large amount of the particles is densely packed with a locally near-hexagonal pattern (see supplemental movies [38]). This strongly hampers or even completely suppresses the flow of particles through the constriction.

In the *oscillatory state*, only sometimes particles of one species manage to pass the constriction. Since the flow of one particle species destroys the force equilibrium at the interface between the particles of both species, the flow is blocked again after a time  $\tau_2$  and it is now easier for particles of the other species to pass the constriction. This leads to a small oscillatory flow through the constriction, where short flows in the positive or negative  $z$  direction and short periods without any flow follow each other so that the sign of  $\langle v \rangle$  changes again and again (see supplemental movies [38]). A related behavior is known from pedestrian streams through a narrow door [32,33,41–43]. The duration  $\tau_2$  of the small unidirectional flows is random with a probability density function  $p(\tau_2/\tau_B)$  that increases for small  $\tau_2$  and decays exponentially for large  $\tau_2$  (see Fig. 3). According to our simulation results,  $p(\tau_2/\tau_B)$  can be described by a function  $p(\tau_2/\tau_B) = c_0(\tau_2/\tau_B)^{c_1} \exp(-c_2\tau_2/\tau_B)$  with fit parameters  $c_0$ ,  $c_1$ , and  $c_2$ . A maximum at intermediate  $\tau_2$  [e.g.,  $\tau_2/\tau_B \approx 75$  for  $b = 2\sigma$  and  $\phi = 0.8$ ; see Fig. 3(a)] designates the characteristic unidirectional-flow duration. For increasing values of  $b$ , the characteristic unidirectional-flow duration and the variance of the probability distribution of  $\tau_2$  decrease [see Fig. 3(b)]. In the *completely jammed state*, in contrast, there is no flow at all and  $\langle v \rangle$  is zero (see supplemental movies [38]).

Both states can follow directly after an asymmetric flow state, alternate repeatedly, and persist for long times. However, we never observed an asymmetric flow state

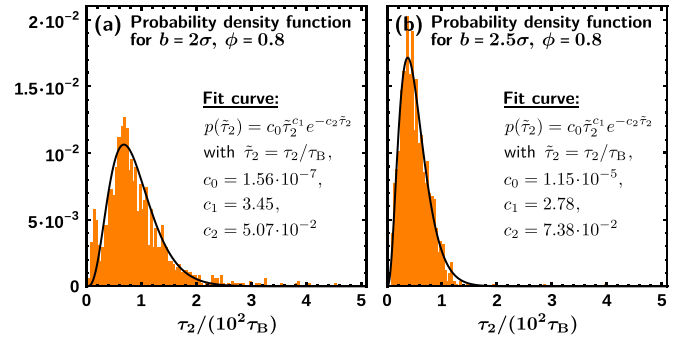


FIG. 3. Histograms and corresponding fit curves for the probability density distribution of the unidirectional-flow duration  $\tau_2$  in the oscillatory state.

following an oscillatory or completely jammed state. The reason is the accumulation of all particles at one constriction in the oscillatory and completely jammed states, whereas there are accumulations of similar size at all constrictions in the asymmetric flow state: When all particles are accumulated at one constriction, the particle flow is so small that the particles can no longer accumulate at other constrictions.

Hence, starting from a homogeneous initial particle distribution, for large  $b$  a persistent symmetric flow state occurs, for sufficiently small  $b$  an asymmetric flow state that can change into an oscillatory or completely jammed state forms, and for  $0 \leq b \lesssim \sigma$  the constrictions are so small that particle flow through them is impossible. The critical value of  $b$  that separates states with clearly nonzero  $|\overline{\langle v \rangle}(b)|$  from those with symmetric flows depends on the particle packing fraction  $\phi$ . It is close to  $\sigma$  for small  $\phi$  and increases with  $\phi$  [see Fig. 4(a)].

#### IV. THEORETICAL CONSIDERATIONS

An approximate expression for the corresponding critical relation of  $b$  and  $\phi$  can be determined by studying the

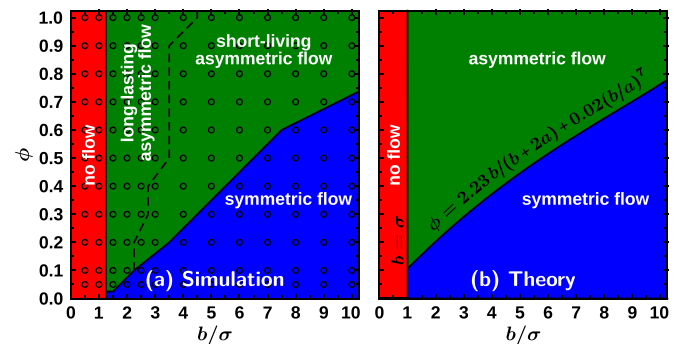


FIG. 4. State diagrams showing the possible occurrence of different flow states obtained by (a) computer simulations and (b) theoretical considerations. Note that an asymmetric flow state can change into an oscillatory or completely jammed state and that these three states therefore occur in the same region of the state diagram. The dashed line separates a region where long-lasting asymmetric flows can be observed, which persist typically for a period of more than  $24\tau_B$ , from a region of only short-living asymmetric flows.

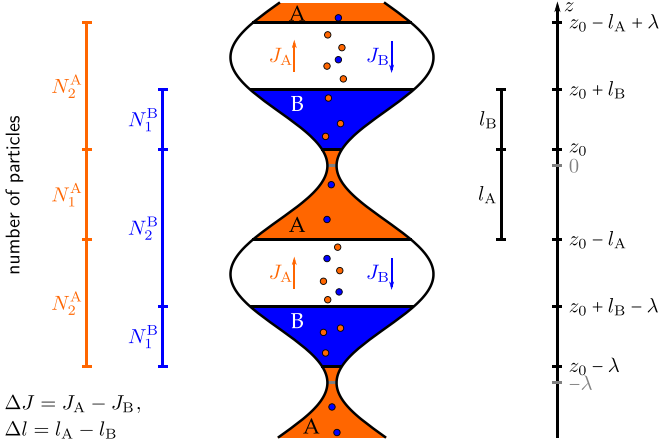


FIG. 5. Schematic illustrating a general asymmetric or symmetric flow state.

stability of asymmetric and symmetric flows. A general flow state, which includes all these spatially periodic flows, is illustrated in Fig. 5. The particles of species A and B accumulate on different sides of the constrictions and are separated by interfaces, but can cross the interfaces with particle current densities  $J_A \geq 0$  and  $J_B \geq 0$ , respectively. Since the system is spatially periodic, it is sufficient to focus on a channel segment of length  $\lambda$ . If  $z_0$  is the interface position in this segment and  $l_A$  and  $l_B$  are the lengths of the channel segments that are occupied mainly by particles of species A and B, respectively, the general flow state can be described by balance equations for the conserved mean numbers  $N_\lambda^A = N_\lambda/2 = 2\phi\lambda(b+2a)/(\pi\sigma^2)$  and  $N_\lambda^B = N_\lambda^A$  of the particles of species A and B in the channel segment of length  $\lambda$ , respectively. We denote the numbers of particles of species A and B in the accumulation areas before and after a constriction by  $N_1^A$  and  $N_1^B$  and the corresponding numbers of nonaccumulated particles that crossed the interface and are on the way to the next accumulation area of the same species by  $N_2^A = N_\lambda^A - N_1^A$  and  $N_2^B = N_\lambda^B - N_1^B$ , respectively. Furthermore, we assume that the particle packing fraction in the accumulation areas is constant and given by  $\phi_{\max} \approx 1$ , that the particles are rigid and have the constant diameter  $\sigma$ , and that the nonaccumulated particles move with the speed  $v_0$ .

Then,  $N_1^A = 2 \int_{z_0-l_A}^{z_0} w(z) dz \phi_{\max}/(\pi\sigma^2/4) - N_2^B l_A/(\lambda - l_B)$  and  $N_2^A = b(\lambda - l_A)(J_A/J_{\max})\phi_{\max}/(\pi\sigma^2/4)$  with the maximum particle current density  $J_{\max} = 4v_0\phi_{\max}/(\pi\sigma^2)$ . Analogous expressions apply to the particles of species B. Together with the continuity conditions  $N_1^A + N_2^A = N_1^B + N_2^B = N_\lambda/2$  and the notation  $W(z) = \int w(z) dz$  this leads to the balance equations

$$2W(z_0) - 2W(z_0 - l_A) - bl_A J_B/J_{\max} + b(\lambda - l_A)J_A/J_{\max} = \lambda(b + 2a)\phi/(2\phi_{\max}), \quad (2)$$

$$2W(z_0 + l_B) - 2W(z_0) - bl_B J_A/J_{\max} + b(\lambda - l_B)J_B/J_{\max} = \lambda(b + 2a)\phi/(2\phi_{\max}) \quad (3)$$

for the particles of species A and B, respectively.

The interface position  $z_0$  and the relative particle flow  $\Delta J = J_A - J_B$  can be time dependent. Their time derivatives are approximately proportional to the force density  $f$ , which the particles of both species exert on the interface. According to the hydrostatic paradox [44],  $f$  is proportional to the segment-length difference  $\Delta l = l_A - l_B$ . This leads to  $\dot{z}_0 \propto \Delta l$  and  $\Delta J \propto \Delta l$ , where the proportionality constants are positive. A stable flow state therefore requires  $\Delta l = 0$ .

We now use Eqs. (2) and (3) to study the existence of flow states with  $\Delta l = 0$ . For  $z_0 = 0$ , such a solution always exists and Eqs. (2) and (3) yield  $\Delta J = 0$ ; i.e., the flow state is *symmetric*. A stable asymmetric flow state is therefore only possible for  $z_0 \neq 0$ . If we increase  $z_0$  (we focus on  $z_0 \geq 0$  for symmetry reasons) and keep  $\Delta J = 0$ ,  $\Delta l$  and thus  $\dot{z}_0$  become positive (see Fig. 5) and the state with  $z_0 = 0$  is unstable. In reality, however, also  $\Delta J$  becomes positive for  $z_0 > 0$  and reduces  $N_1^A$  and thus  $\Delta l$  and  $\dot{z}_0$ . The sign of  $\dot{z}_0$  for  $z_0 \approx 0$  and thus the stability of the symmetric flow state therefore depend on the parameters of the system. If  $\Delta J$  is sufficiently small for  $z_0 \approx 0$ , there exists another solution of Eqs. (2) and (3) for  $\Delta l = 0$ , where  $z_0 > 0$  and  $\Delta J > 0$ . This solution is stable and corresponds to an *asymmetric* flow state.

By considering different values of  $b$  and  $\phi$  and numerically searching for corresponding solutions of Eqs. (2) and (3) with  $\Delta l = 0$  and  $z_0 > 0$ , one obtains the critical relation of  $b$  and  $\phi$ . If we focus on flow states where only the particles of one species are flowing and approximate their current density by  $J_{\max}$ , the critical relation can be approximated by the fit function  $\phi = 2.23b/(b + 2a) + 0.02(b/a)^7$  [see Fig. 4(b)]. This result is in good agreement with our simulations (see Fig. 4).

## V. RELEVANCE OF THE RESULTS

Our results are applicable not only to the model given by the Langevin equations (1), but also to real systems. In this section we address possible experimental realizations of the model and show that our results are relevant also for other systems.

### A. Experimental realization of our model

Our model can be realized in experiments with a binary suspension of colloidal particles in a microfluidic channel. There are different possible ways to drive two species of such particles in opposite directions through the channel (see Fig. 6). These methods include the application of time-dependent light fields to drive the particles, which is already a well-established technique, and self-propelled particles (see below).

A possible way is to use optically nonabsorbing particles with different frequency-dependent refractive indices  $n_1(\nu)$  and  $n_2(\nu)$  and to choose the surrounding liquid in such a way that its refractive index matches  $n_1(\nu)$  and  $n_2(\nu)$  at different frequencies  $\nu_1$  and  $\nu_2$ , respectively. Then, inhomogeneous light fields with frequencies  $\nu_1$  and  $\nu_2$  have an effect only on particles of one species each. If the intensity profiles of the two light fields have a saw-tooth shape and travel in opposite directions along the channel, the particles are oppositely driven through the channel by gradient forces [see Fig. 6(a)].

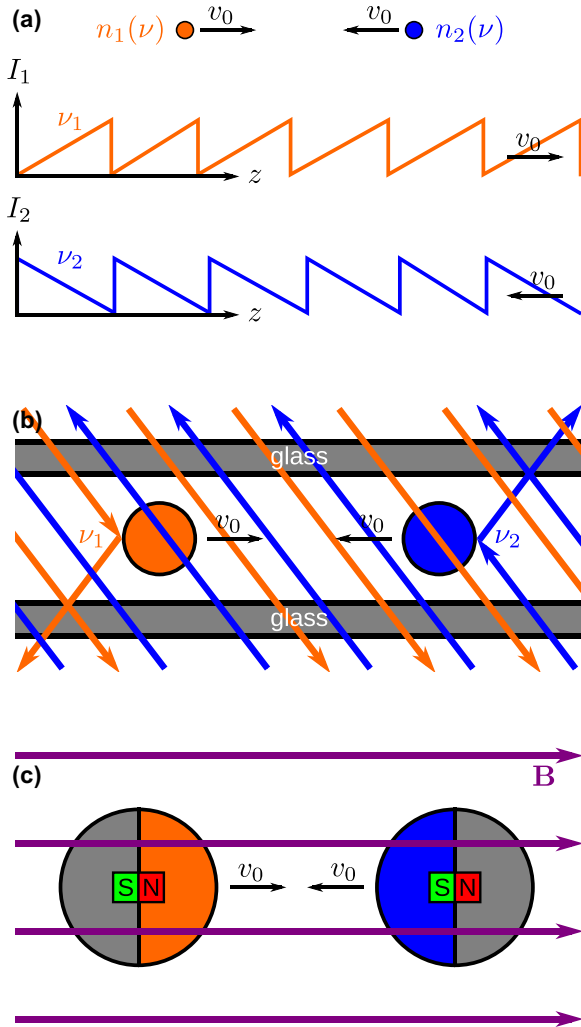


FIG. 6. Different possible ways to drive two species of colloidal particles in opposite directions through a surrounding liquid. (a) Optically nonabsorbing particles with different frequency-dependent refractive indices  $n_1(\nu)$  and  $n_2(\nu)$  in light fields with different frequencies  $\nu_1$  and  $\nu_2$  and oppositely traveling saw-tooth-shaped intensity profiles  $I_1(z)$  and  $I_2(z)$ . (b) Cross section of a quasi-two-dimensional channel with particles that reflect light of frequencies  $\nu_1$  and  $\nu_2$  but transmit light of frequencies  $\nu_2$  and  $\nu_1$ , respectively, under illumination with frequencies  $\nu_1$  and  $\nu_2$  from opposite directions. (c) Self-propelled particles with small magnetic cores whose magnetizations are parallel and antiparallel to the self-propulsion direction, respectively, are oppositely oriented by a homogeneous external magnetic field with flux density  $\mathbf{B}$ .

Another possibility to drive colloidal particles in opposite directions through an effectively two-dimensional channel is to use particles of different materials that reflect light of frequencies  $\nu_1$  and  $\nu_2$  but transmit light of frequencies  $\nu_2$  and  $\nu_1$ , respectively. If a suspension of such particles is illuminated in the direction of the channel axis by light with the frequency  $\nu_1$  and in the opposite direction by light with the frequency  $\nu_2$ , the particles of different species are light-pressure driven in opposite directions through the channel [see Fig. 6(b)].

A further alternative is to use self-propelled particles [45–47] with small magnetic cores. If the particles are much

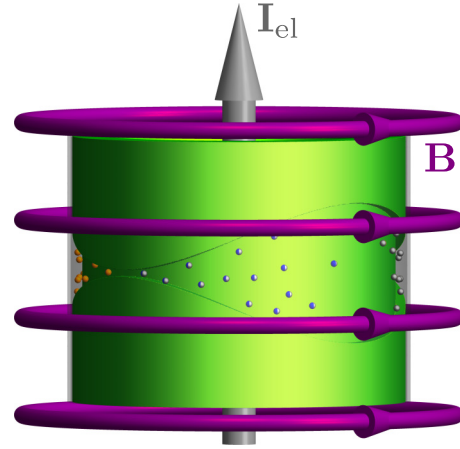


FIG. 7. Sketch of an experimental realization of our model with two species of self-propelled colloidal particles with small magnetic cores that are aligned in opposite directions by an external magnetic field with flux density  $\mathbf{B}$  generated by an axial electric current  $\mathbf{I}_{el}$ . The average mass densities of the particles equal the mass density of the surrounding liquid in order to avoid an influence of gravity on the particle motion.

larger than their cores, they can be oriented by an external magnetic field while magnetic interactions of different particles can be neglected. Using two species of such particles, where the magnetizations of the cores are parallel and antiparallel to the self-propulsion direction of the particles, respectively, and a homogeneous external magnetic field parallel to the channel axis leads to a system where the particles of both species propel themselves forward in opposite directions through the channel [see Figs. 6(c) and 7].

**B. Applicability of our model to other systems**

The basic behavior of our colloidal model is not sensitive to the details of the model. This makes our qualitative results relevant for a large number of different real systems including even macroscopic ones. In the following, we demonstrate for three different examples that the main results of our model do not change if the model is modified.

*1. Space-dependent diffusion coefficient*

We first consider a system with a space-dependent diffusion coefficient  $D(x, z)$ . For this purpose, we replace the constant diffusion coefficient  $D_T$  in the Langevin equations (1) by the position-dependent diffusion coefficient

$$D(x, z) = \frac{D_T}{6} [4 - \tanh(4 - w(z)/\sigma - x/\sigma) - \tanh(4 - w(z)/\sigma + x/\sigma)], \quad (4)$$

which equals  $D_T$  far away from the walls and decreases near the walls. Using this space-dependent diffusion coefficient, we repeated the Brownian dynamics simulations corresponding to the parameter combinations marked by yellow circles in Fig. 8.

As expected, we observed the same flow states as in our original simulations described in Sec. III. This confirms that such a space-dependent diffusion coefficient can only slightly change the state diagram of our model.

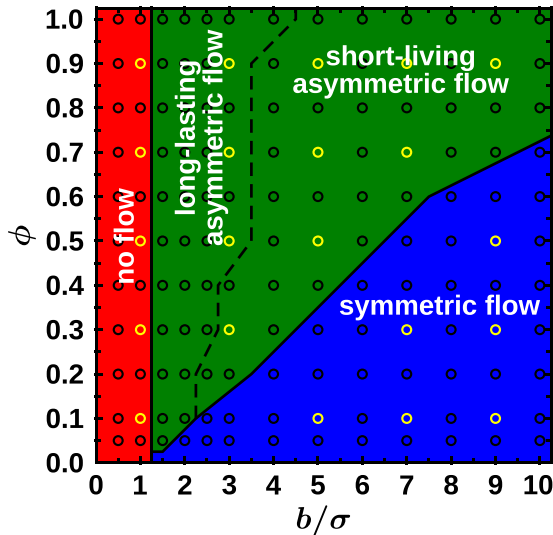


FIG. 8. State diagram from Fig. 3(a), but now with the parameter combinations where we carried out additional simulations marked by yellow circles.

### 2. Different particle interactions

Next, we consider particle-particle interactions with an attractive contribution given by the pair-interaction potential

$$U_{\text{att}}(r) = \frac{U_0\sigma}{r} (5e^{-7r/\sigma} - 2e^{-6r/\sigma}). \quad (5)$$

This potential has a minimum value of about  $-2k_B T$  and satisfies the equation  $-U'_{\text{att}}(r) = F_{\text{ext}}$  for  $r \approx \sigma$ , i.e.,  $U_{\text{att}}(r)$  is consistent with the definition of  $\sigma$ . On this basis, we addressed two situations. In the first one, we used the potential  $U_{\text{att}}(r)$  instead of  $U(r)$  for all particle-particle interactions; i.e., we considered two species of oppositely driven repulsive particles with an attractive contribution in the interactions. In the second situation, in contrast, we used the purely repulsive potential  $U(r)$  for the interactions of particles of the same species but the potential  $U_{\text{att}}(r)$  for the interactions of particles of different species. This corresponds to soft charged particles, where the particles of the two species have opposite charges. For both situations, we carried out simulations corresponding to the parameter combinations marked by yellow circles in Fig. 8. In these simulations we observed that the attractive component in the particle-particle interactions fosters the accumulation of

the particles at the constrictions of the channel. This reduces the stability and duration of the asymmetric flow states and shifts the curve that separates asymmetric from symmetric flow states in Fig. 8 to the left for  $\phi > 0.1$ . Nevertheless, the qualitative structure of the state diagram is unchanged. This suggests that our qualitative results are not sensitive to the details of the particle-particle interactions in our model.

### 3. Different channel lengths

We also carried out additional simulations for systems with different channel lengths  $L = \lambda, \dots, 8\lambda$ . Interestingly, the four different flow states described in Sec. III can be observed in all these cases. For  $L = \lambda$ , the asymmetric flow state and the oscillatory flow state can be combined to a single flow state. In contrast, for  $L > 2\lambda$  we also observed new flow states that cannot occur in systems with  $L/\lambda \leq 2$ .

## VI. CONCLUSIONS

In summary, we have studied the flow and clogging behavior of oppositely driven colloidal particles in a periodic channel with constrictions. We have shown that as a consequence of spontaneous symmetry breaking, even in an initially completely symmetric system partial clogging, where the particles of one species are flowing and the other particles are clogging, can occur. In addition, we have observed self-organized oscillations in clogging and unclogging of the two species. Our work demonstrates that and how the flow state of a corresponding system can be steered by tuning the constriction size and particle packing fraction appropriately. These results are interesting from a statistical physics point of view and relevant also for many real systems in various fields ranging from nanofluidics to crowd management. In the future, our system could be directly realized in experiments with suspensions of two species of oppositely light-driven colloidal particles or with self-propelled colloidal core-shell particles with small magnetic cores that are oppositely aligned by an external magnetic field.

## ACKNOWLEDGMENTS

This work was funded in part by the ERC Advanced Grant INTERCOCOS (Grant No. 267499). R.W. gratefully acknowledges financial support through a Return Fellowship (WI 4170/2-1) from the Deutsche Forschungsgemeinschaft (DFG).

[1] J. C. T. Eijkel and A. van den Berg, *Microfluidics Nanofluidics* **1**, 249 (2005).  
 [2] R. B. Schoch, J. Han, and P. Renaud, *Rev. Mod. Phys.* **80**, 839 (2008).  
 [3] L. Bocquet and E. Charlaix, *Chem. Soc. Rev.* **39**, 1073 (2010).  
 [4] U. M. B. Marconi, P. Malfaretti, and I. Pagonabarraga, *J. Chem. Phys.* **143**, 184501 (2015).  
 [5] M. A. Fallah, V. M. Myles, T. Krüger, K. Sritharan, A. Wixforth, F. Varnik, S. W. Schneider, and M. F. Schneider, *Biomicrofluidics* **4**, 024106 (2010).  
 [6] H. Noguchi, G. Gompfer, L. Schmid, A. Wixforth, and T. Franke, *Europhys. Lett.* **89**, 28002 (2010).

[7] M. O. Bernabeu, R. W. Nash, D. Groen, H. B. Carver, J. Hetherington, T. Krüger, and P. V. Coveney, *Interface Focus* **3**, 0120094 (2013).  
 [8] R. D. Peacock, E. D. Kuligowski, and J. D. Averill, *Pedestrian and Evacuation Dynamics*, 1st ed. (Springer-Verlag, Berlin, 2011).  
 [9] J. Dzubiella and J.-P. Hansen, *J. Chem. Phys.* **122**, 234706 (2005).  
 [10] H. M. Wyss, D. L. Blair, J. F. Morris, H. A. Stone, and D. A. Weitz, *Phys. Rev. E* **74**, 061402 (2006).  
 [11] D. Genovese and J. Sprakel, *Soft Matter* **7**, 3889 (2011).

- [12] C. Kreuter, U. Siems, P. Nielaba, P. Leiderer, and A. Erbe, *Eur. Phys. J. Spec. Top.* **222**, 2923 (2013).
- [13] A. V. Ivlev, H. Löwen, G. E. Morfill, and C. P. Royall, *Complex Plasmas and Colloidal Dispersions: Particle-Resolved Studies of Classical Liquids and Solids*, 1st ed., Series in Soft Condensed Matter Vol. 5 (World Scientific, Singapore, 2012).
- [14] S. E. Hulme, W. R. DiLuzio, S. S. Shevkoplyas, L. Turner, M. Mayer, H. C. Berg, and G. M. Whitesides, *Lab. Chip* **8**, 1888 (2008).
- [15] E. Altshuler, G. Miño, C. Pérez-Penichet, L. del Río, A. Lindner, A. Rousselet, and E. Clément, *Soft Matter* **9**, 1864 (2013).
- [16] J. K. Patnaik, B. S. Das, S. K. Mishra, S. Mohanty, S. K. Satpathy, and D. Mohanty, *Am. J. Trop. Med. Hyg.* **51**, 642 (1994).
- [17] I. Zuriguel, A. Janda, A. Garcimartín, C. Lozano, R. Arévalo, and D. Maza, *Phys. Rev. Lett.* **107**, 278001 (2011).
- [18] C. C. Thomas and D. J. Durian, *Phys. Rev. Lett.* **114**, 178001 (2015).
- [19] D. Helbing, I. Farkas, and T. Vicsek, *Nature (London)* **407**, 487 (2000).
- [20] A. Kirchner, K. Nishinari, and A. Schadschneider, *Phys. Rev. E* **67**, 056122 (2003).
- [21] I. Zuriguel, D. R. Parisi, R. C. Hidalgo, C. Lozano, A. Janda, P. A. Gago, J. P. Peralta, L. M. Ferrer, L. A. Pugnaloni, E. Clément, D. Maza, I. Pagonabarraga, and A. Garcimartín, *Sci. Rep.* **4**, 7324 (2014).
- [22] A. Garcimartín, J. M. Pastor, L. M. Ferrer, J. J. Ramos, C. Martín-Gómez, and I. Zuriguel, *Phys. Rev. E* **91**, 022808 (2015).
- [23] M. Muramatsu, T. Irie, and T. Nagatani, *Physica A (Amsterdam, Neth.)* **267**, 487 (1999).
- [24] D. Helbing, I. J. Farkas, and T. Vicsek, *Phys. Rev. Lett.* **84**, 1240 (2000).
- [25] J. Dzubiella, G. P. Hoffmann, and H. Löwen, *Phys. Rev. E* **65**, 021402 (2002).
- [26] R. R. Netz, *Europhys. Lett.* **63**, 616 (2003).
- [27] K. R. Sütterlin, A. Wysocki, A. V. Ivlev, C. Räh, H. M. Thomas, M. Rubin-Zuzic, W. J. Goedheer, V. E. Fortov, A. M. Lipaev, V. I. Molotkov, O. F. Petrov, G. E. Morfill, and H. Löwen, *Phys. Rev. Lett.* **102**, 085003 (2009).
- [28] T. Vissers, A. van Blaaderen, and A. Imhof, *Phys. Rev. Lett.* **106**, 228303 (2011).
- [29] T. Vissers, A. Wysocki, M. Rex, H. Löwen, C. P. Royall, A. Imhof, and A. van Blaaderen, *Soft Matter* **7**, 2352 (2011).
- [30] S. Nowak and A. Schadschneider, *Phys. Rev. E* **85**, 066128 (2012).
- [31] B. Heinze, U. Siems, and P. Nielaba, *Phys. Rev. E* **92**, 012323 (2015).
- [32] D. Helbing, I. J. Farkas, P. Molnar, and T. Vicsek, *Pedestrian and Evacuation Dynamics* (Springer-Verlag, Berlin, 2001), Chap. 2, pp. 21–58.
- [33] D. Helbing, *Comput. Mater. Sci.* **30**, 180 (2004).
- [34] B. Hille, *Ion Channels of Excitable Membranes*, 3rd ed. (Sinauer Associates, Sunderland, 2001).
- [35] F. M. Ashcroft, *Ion Channels and Disease*, 1st ed. (Academic Press, San Diego, 1999).
- [36] The particle packing fraction  $\phi = N_\lambda(\pi\sigma^2/4)/[\lambda(b+2a)]$  is defined via the effective particle diameter  $\sigma$ .
- [37] M. P. Allen and D. J. Tildesley, *Computer Simulation of Liquids*, 1st ed. (Oxford University Press, Oxford, UK, 1989).
- [38] See Supplemental Material at <http://link.aps.org/supplemental/10.1103/PhysRevE.94.052606> for movies.
- [39] In contrast to a ratchet current [48], this rectified particle transport does not require a spatially or temporally symmetry-broken system.
- [40] We define the characteristic flipping time  $\tau_1$  as the first zero of the velocity autocorrelation function  $C(\tau) = \int_{t_0}^{t_{\max}} \langle v(t)v(t+\tau) \rangle / \langle v(t)^2 \rangle dt / (t_{\max} - t_0)$  with  $t_0 = 500\tau_B$  and  $t_{\max} = 10^4\tau_B$  for  $1.5\sigma \leq b \leq 2.5\sigma$  and  $t_{\max} = 10^3\tau_B$  otherwise.
- [41] D. Helbing and P. Molnár, *Phys. Rev. E* **51**, 4282 (1995).
- [42] D. Helbing, *Rev. Mod. Phys.* **73**, 1067 (2001).
- [43] D. Helbing, P. Molnár, I. J. Farkas, and K. Bolay, *Environ. Plan. B* **28**, 361 (2001).
- [44] W. H. Besant, *Elementary Hydrostatics*, 5th ed. (Deighton, Bell, and Co., Cambridge, 1873).
- [45] S. J. Ebbens and J. R. Howse, *Soft Matter* **6**, 726 (2010).
- [46] M. C. Marchetti, J. F. Joanny, S. Ramaswamy, T. B. Liverpool, J. Prost, M. Rao, and R. A. Simha, *Rev. Mod. Phys.* **85**, 1143 (2013).
- [47] W. Wang, W. Duan, S. Ahmed, T. E. Mallouk, and A. Sen, *Nano Today* **8**, 531 (2013).
- [48] P. Hänggi and F. Marchesoni, *Rev. Mod. Phys.* **81**, 387 (2009).